Macromolecular Rapid Communications
www.mrc-journal.de

Understanding the Critical Role of Sequential Fluorination of Phenylene Units on the Properties of Dicarboxylate Bithiophene-Based Wide-Bandgap Polymer Donors for Non-Fullerene Organic Solar Cells

*Gururaj P. Kini, Eui Jin Lee, Sung Jae Jeon, and Doo Kyung Moon**

Design and development of wide bandgap (WBG) polymer donors with low-lying highest occupied molecular orbitals (HOMOs) are increasingly gaining attention in non-fullerene organic photovoltaics since such donors can synergistically enhance power conversion efficiency (PCE) by simultaneously minimizing photon energy loss (E_{loss}) and enhancing the spectral response. In this contribution, three new WBG polymer donors, P1, P2, and P3, are prepared by adding phenylene cores with a different number of fluorine (F) substituents (n = 0, 2, and 4, respectively) to dicarboxylate bithiophene-based acceptor units. As predicted, fluorination effectively aides in the lowering of HOMO energy levels, tailoring of the coplanarity and molecular ordering in the polymers. Thus, fluorinated P2 and P3 polymers show higher coplanarity and more intense interchain aggregation than P1, leading to higher charge carrier mobilities and superior phase-separated morphology in the optimized blend films with IT-4F. As a result, both P2:IT-4F and P3:IT-4F realize the best PCEs of 6.89% and 7.03% (vs 0.16% for P1:IT-4F) with lower E_{loss} values of 0.65 and 0.55 eV, respectively. These results signify the importance of using phenylene units with sequential fluorination in polymer backbone for modifying the optoelectronic properties and realizing low E_{loss} values by synergistically lowering the HOMO energy levels.

1. Introduction

Organic solar cells (OSCs) are considered a front runner among emerging next-generation low-cost and clean energy harvesting technologies owing to their unique benefits in the fabrication of highly flexible, semi-trasparent, low-cost, and weightless large-area photovoltaic panels using simple solution-processable roll-to-roll fabrication methods.[1–6,72] Over the last 5 years, the design and development of novel photovoltaic materials have been subjects of intense focus and several reliable molecular strategies, including chemical and structural modification methods, have been successfully developed and extensively tested.[2,3,7–12] In particular, there have been rapid advancements in the rational design of low-bandgap non-fullerene fused-ring small-molecule electron acceptors (NFAs or FREAs),[11–16] which yielded easy tailoring of optical, electrochemical, and electron mobilities (μ_e), and good charge transport properties compared to fullerene acceptors. Consequently, the use of FREAs in combination with appropriate wide-bandgap (WBG) polymer donors has boosted the power conversion efficiencies (PCEs) of single-junction OSCs to 14–17%.[6,17–22] It is well-known that the PCE of an OSC depends on three key parameters, that is, short-circuit current density (J_{sc}), open-circuit voltage (V_{oc}), and fill factor (FF). Hence, the simultaneous maximization of all three factors is critical for the development of efficient OSCs. Although many successful OSCs demonstrate outstanding PCEs by affording superior J_{sc} values of ≈85% that approach the theoretical maximum obtained from external quantum efficiency (EQE) profiles[23–26] and remarkable FF values over 80%,[27,28] but they show relatively low V_{oc} values due to the low-lying lowest unoccupied molecular orbitals (LUMO) of near-infrared NFAs, which negatively affects the photon energy loss ($E_{loss} = E_g - qV_{OC}$, where E_g is the optical bandgap of the main light absorber and q is the elementary charge).[29–31] Besides, recent developments in new donor materials with deep-lying highest occupied molecular orbitals (HOMOs) suggest that this approach could reliably enhance the efficiency of NF-OSCs, since OSCs based on this type of polymers exhibit a superior trade-off between V_{oc} and J_{sc} by greatly suppressing E_{loss}.[17–22,32–34]

In the OSC research community, polythiophene (PT)-based donors have generated a considerable degree of interest, mainly because of their high scalability at low cost.[34–37] In particular, with the addition of two carboxylate substituents to the side position of 2,2′-bithiophene unit, the HOMO energy levels are consecutively lowered, and the coplanarity and solubility of the polymer backbone are successively enhanced, leading to a remarkable enhancement in PCE in the corresponding polymers.[34,38–41] For example, Hou et al. successfully broke

Dr. G. P. Kini, Dr. E. J. Lee, Dr. S. J. Jeon, Prof. D. K. Moon
Nano and Information Materials (NIMs) Laboratory
Department of Chemical Engineering
Konkuk University
120 Neungdong-ro, Seoul 05029, Republic of Korea
E-mail: dkmoon@konkuk.ac.kr

DOI: 10.1002/marc.202000743

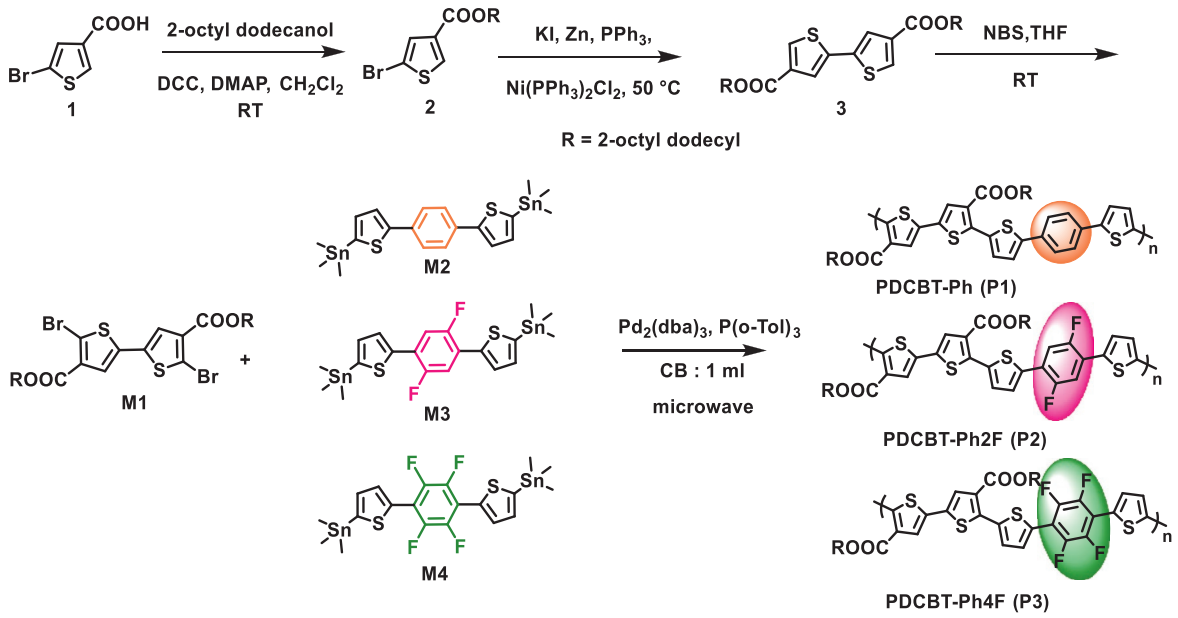

Scheme 1. Synthesis routes of monomer M1 and polymers P1, P2, and P3.

the 10% PCE barrier for PT-based donors by synthesizing a PDCBT polymer that demonstrated efficiency of 10.16% with an excellent V_{OC} of 0.94 V with an ITIC acceptor.[42] In their next study, the same group further introduced fluorine (F) atoms into the PDCBT backbone to form PDCBT-2F, which showed a 0.36 eV deeper HOMO versus PDCBT and optimized PDCBT-2F:IT-M-based OSCs that afforded a higher V_{OC} of 1.13 V and an efficiency of 6.6%.[43] Motivated by these successes, Geng et al. further studied the effects of halogen inclusion in PDCBT molecular design by varying the number (1 or 2) and type of halogen (F or chlorine [Cl]) substituents in the bithiophene units to form a series of PT-based polymers, among which PDCBT-F and PDCBT-Cl afforded the highest PCEs of 10.85% and 12.38%, respectively, with V_{OC} values above 0.93 V.[34] These results suggest that [2,2′-bithiophene]-4,4′-dicarboxylate (DCBT) is one of the promising monomer units for the design of WBG donor materials. However, despite the impressive PCEs of these polymers, the synthetic costs of the halogenated bithiophene monomers are high because of more synthetic steps, tedious purification procedures and lower reaction yield involved in the introduction of halogen substituents in bithiophene units (Scheme S1, Supporting Information). Therefore, further exploration of new PT-based polymer donors with HOMO energy levels and lower synthetic cost is an interesting topic of research that may lead to the development of highly efficient, scalable, and inexpensive polymer donors for OSCs.

Among the various emerging weak electron-deficient units, phenylene moieties with high aromatic resonance energy are considered an excellent choice for lowering HOMOs and, thus, increasing V_{OC}.[44,45] Importantly, there are four vacant positions in the phenylene core which are readily available for structural modification. This offers an excellent opportunity to optimize the optoelectronic properties and aggregation behavior of the resulting materials. The F atom, which has the highest electronegativity among the halogens, is highly studied and considered a smart choice for synergistic enhancement of the absorption coefficient and coplanarity via enhanced F-induced inter/intramolecular interactions, crystallinity, and charge carrier mobility, and suppression of the HOMO energy levels in resulted photoabsorbant materials, thus providing excellent PCEs in both fullerene and NF-OSCs.[6,46–54] Although a few previous reports have indicated drawbacks of fluorinated monomers, such as high synthetic cost, low yields during fluorination exchange reaction, and the need for complex purification procedures;[55] however, fluorinated phenylene moieties are cheap and commercially available and functionalization of them involves few synthetic steps and easy purification as shown in Scheme S1, Supporting Information. Moreover, there are various successful examples of donor–acceptor polymers with fluorinated phenylene moieties that were previously reported for organic photovoltaic applications, which illustrates their potential for the development of efficient photoabsorbent materials.[41,44,45,48,56]

Considering the abovementioned facts, we propose the design of a series of new WBG polymers, poly-{bis(2-octyldodecyl) 5″-methyl-5-(4-(5-methylthiophen-2-yl)phenyl)-[2,2′:5′,2″-terthiophene]-3′,4″-dicarboxylate}(PDCBT-Ph or P1), poly-{bis(2-octyldodecyl) 5-(2,5-difluoro-4-(5-methylthiophen-2-yl) phenyl)-5″-methyl-[2,2′:5′,2″-terthiophene]-3′,4″-dicarboxylate} (PDCBT-Ph2F or P2), and poly-{ bis(2-octyldodecyl) 5″-methyl-5-(2,3,5,6-tetrafluoro-4-(5-methylthiophen-2-yl)phenyl)-[2,2′:5′,2″-terthiophene]-3′,4″-dicarboxylate}(PDCBT-Ph4F or P3) with deep HOMO energy levels. The newly designed polymers were created by inserting a phenylene core with different numbers of F substituents (n = 0, 2, and 4, respectively) into the PDCBT backbone (**Scheme 1**). The effects of the different extents of fluorination on the absorption, energy level, molecular ordering, and charge transport properties of the resulting copolymers were systematically studied. As expected, from the F-less P1 to the difluoro analogue P2 and then to the tetrafluoro analogue P3, the copolymers demonstrated

progressive decrease in frontier energy levels, higher absorption coefficients, and strong aggregation behavior with shorter π–π stacking distances. Moreover, when mixed with the IT-4F acceptor, both P2- and P3-based OSCs displayed more complementary absorption with the IT-4F acceptor, well-balanced carrier mobilities and excellent surface morphology, which eventually leads to efficiencies of 6.89% and 7.03% with low E_{loss}. Thus, this set of copolymers provide valuable guidelines for designing the WBG donor materials with enhanced voltage and minimized E_{loss} by integrating synergistic effects of sequential fluorination.

2. Result and Discussion

The new WBG polymers P1–P3 were prepared using the Stille coupling reaction between bis(2-octyldodecyl)-5,5′-dibromo-[2,2′-bithiophene]-4,4′-dicarboxylate monomer (M1) and corresponding dithienyl-substituted phenyl compounds with different numbers of F substituents (M2–M4), as presented in Scheme 1. M1 was synthesized in three steps starting from 5-bromothiophene-3-carboxylic acid (1). First, 2 was prepared with a 70% yield by the esterification of compound 1 using the Steglich esterification procedure using 2-octyl-1-dodecanol and, dicyclohexylcarbodiimide (DCC) and 4-dimethylaminopyridine (DMAP) as the coupling agent and catalyst, respectively. Then, a homocoupling of 2 in the presence of potassium iodide (KI), zinc powder (Zn), triphenylphosphine (PPh_3), and $Ni(PPh_3)_2Cl_2$ at 50 °C afforded bis(2-octyldodecyl) DCBT (3) with a 70% yield. Finally, the bromination of compound 3 using *N*-bromosuccinimide (NBS) in chloroform (CF) and trifluoroacetic acid (1:1) gave monomer M1 with a yield of over 70%. Monomers M2–M4 were synthesized according to a previous report;[45] detailed synthesis procedures for M1 and P1–P3 can be found in the Supporting Information. Generally, polymers with F substituents exhibit lower solubility than those without; therefore, larger alkyl chains were introduced to M1 to guarantee the sufficient solubility of the final polymers for solution processing. Thus, all newly synthesized polymers showed good solubility in organic solvents such as CF, chlorobenzene (CB), and o-dichlorobenzene. Using gel-permeation chromatography (GPC) against polystyrene standards, the number-averaged molecular weight (M_n) was estimated to be 25.7, 32.7, and 27.8 kDa with a corresponding polydispersity index of 1.63, 1.75, and 1.74, respectively, for P1, P2, and P3.

To evaluate the influence of sequential fluorination of the dithienyl-substituted phenyl unit on the torsional energy barrier in the polymer backbone and its frontier molecular orbitals (FMO) energy levels, theoretical calculations were performed using density functional theory (DFT) at the B3LYP/6-31G(d) level in Gaussian 09 (Figure S1, Supporting Information). To minimize complexity and save time, the alkyl chain on the polymer backbone was replaced with methyl substituents and the calculations were carried out based on two repeating polymer units. The results showed that polymers P2 and P3, with two and four F atoms, respectively, showed smaller torsion angles between the thiophene and phenyl moieties (θ_2/θ_3 = 22.85/22.41°, 0.65/1.22°, and 2.05/4.27° for P1, P2, and P3, respectively) than P1, which lacked F substituents (Table S1, Supporting Information). Whereas, all of the polymers exhibited similar torsion angles (θ_1/θ_4 of ≈22.16–24.6°) between thiophene and adjacent carboxylate-substituted thiophene units. These results were ascribed from the weak covalent F–S intramolecular interactions facilitated by fluorination, which resulting in decreased F–S distances (2.75 and 2.72 Å for P2 and P3, respectively) compared to the actual distance of 3.27 Å (calculated by combining the van der Waals radii of F and S atoms).[34,48,52,57] Moreover, the side view showing an increase in the bond length of the polymer backbone (L_{bond} for P1, P2, and P3 = 39.60, 40.05, and 39.99 Å, respectively) suggests that fluorination can improve effective conjugation and structural planarity, which could promote more orderly interchain packing, thereby affecting morphology and increasing the charge transport efficiency of the solar cells. However, P3, with four F substituents, demonstrated slightly increased torsion profiles compared to P2; this is because of the larger van der Waals radius of F than H. As shown in the FMO energy diagrams (Figure S1, Supporting Information), all of the polymers in this series demonstrated similar electron distributions, with HOMO and LUMO well-distributed along the entire backbone, but their energy levels were synergistically downshifted depending on the number of inserted F substituents due to the strong electronegativity of the F atom.

The normalized ultraviolet–visible (UV–vis) absorption profiles of the newly synthesized polymers in CF solution and the thin film states are demonstrated in **Figure 1**a,b; the relevant optical properties are presented in **Table 1**. In solution, the three polymers showed absorption profiles with absorption maxima (λ_{abs}) located between 453–566 nm, whereas in the thin film state, λ_{abs} were red-shifted due to enhanced interchain organization. However, the absorption profile of P1 without F substituents displayed largely blue-shifted absorption spectra without any obvious shoulder peak in both the solution and film states compared to P2 and P3, suggesting that the weakest interchain aggregation exists in P1, which may lead to decreased interchain interactions and poor molecular packing. Such absorption features can be ascribed to the absence of F-induced non-covalent interactions, resulting in larger backbone torsion, as shown in the DFT calculations. Therefore, the insertion of difluoro- and tetrafluoro-phenylene units with F substituents facilitated higher planarity and stronger aggregation tendencies, resulting in a remarkable enhancement of vibronic peaks in P2 and P3 and indicating that both polymers have higher interchain aggregation than P1. Furthermore, the molar extinction coefficients (ε) of the polymers also increased in the order of $4.7 \times 10^4 > 5.4 \times 10^4 > 5.7 \times 10^4$ M^{-1} cm^{-1}, respectively, for P1, P2, and P3, thereby emphasizing that insertion of F atoms aids in the enhancement of ε via the high coplanarity and improved interchain ordering in the backbone of the fluorinated polymer.[48,58] The optical bandgaps (E_g^{opt}), which were calculated from the respective absorption onset values (λ_{onset}) using the equation $E_g^{opt} = 1240/\lambda_{onset}$, were 2.13 (P1), 1.96 (P2), and 2.00 eV (P3).

To further elucidate the electrochemical properties of these new polymers, the HOMO and LUMO energy levels of the polymers against the ferrocene standards were measured using cyclic voltammetry. The cyclic voltammetry profiles of the polymers are depicted in Figure 1c and the parameters extracted

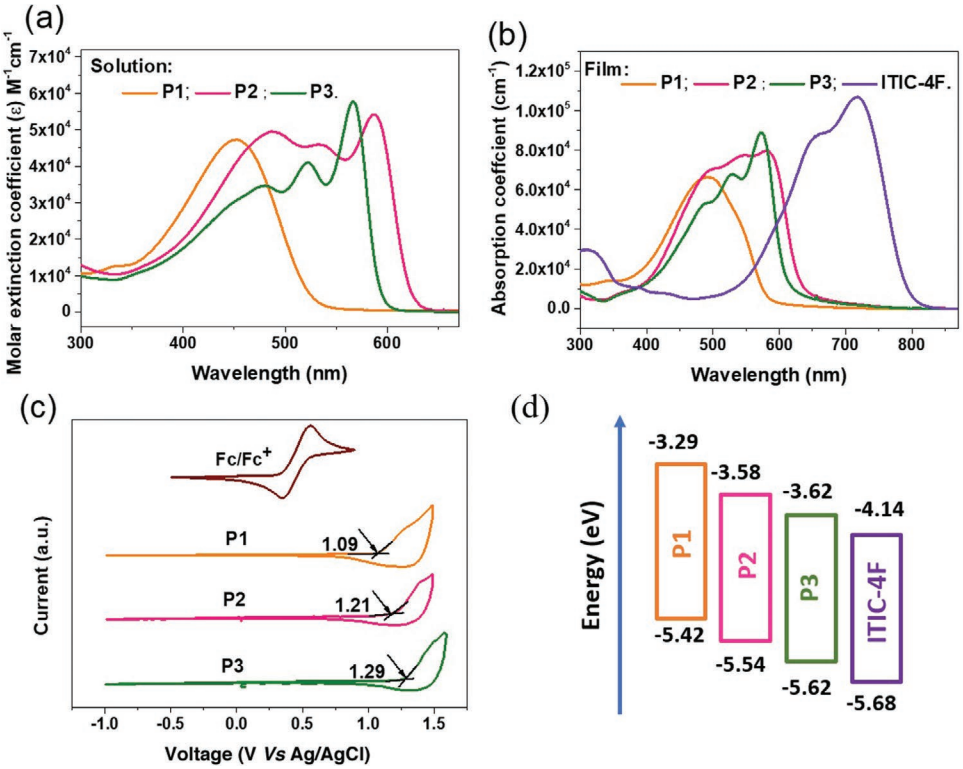

Figure 1. a) UV–vis absorption spectra of the three polymers in chloroform solution at room temperature, b) Absorption coefficient spectra of polymers and IT-4F in the thin-film state, c) Cyclic voltammograms and d) Schematic illustration of the energy level alignment of the active layer components.

from these images are summarized in Table 1. From the onsets of oxidation/reduction potentials, the HOMO/LUMO of P1, P2, and P3 were estimated to be −5.42/−3.29, −5.54/−3.58, and −5.62/−3.62 eV, respectively. As predicted, due to the insertion of electrophilic F substituents with higher electronegativity, from P1 to P2 and then to P3, both HOMO and LUMO energy levels were reduced; these results were validated by the DFT calculation results. Thus, the presence of the carboxylate group and the extent of fluorination have a synergistic influence on lowering the HOMO and are thus presumed to yield higher V_{oc} in the order P3 > P2 > P1 in solar devices. Moreover, all three polymers demonstrated complementary absorption and well-aligned energy level matching with a well-proven IT-4F acceptor (Figure 1b,d). Thus, IT-4F was used as an acceptor unit to test the polymers. Moreover, all three polymers also showed good thermal stability with a decomposition temperature (T_d) of 365, 372 and 388 °C, respectively, for P1–P3, as estimated using thermogravimetric analysis (Figure S2, Supporting Information).

X-ray diffraction (XRD) analysis was used to obtain more information on the effect of sequential fluorination on molecular orientation and packing in the pristine polymers. **Figure 2** represents the in-plane direction (q_{xy}) and out-of-plane direction (q_z) profiles of the XRD images obtained from pristine P1–P3 polymers; the packing parameters extracted from these images are listed in Table S2, Supporting Information. All of the polymers exhibited intense (100) Braggs diffraction (located at 3.59–3.78 Å^{-1}) along both the q_{xy} and q_z directions, which corresponds to a lamellar stacking d-spacing of ≈23.35–24.57 Å. Likewise,

Table 1. Number-averaged molecular weights (M_n) with the corresponding polydispersity index (PDI), photophysical, and electrochemical properties of the polymers.

Polymer	M_n [kDa]/PDI[a)]	Photophysical properties					Electrochemical properties		
		λ_{max} [nm], solution	ε [10⁴] [M⁻¹ cm⁻¹][b)]	λ_{max} [nm], thin film	λ_{onset} [nm], thin film	E_g^{opt} [eV][c)]	E_{ox}^{onset} [V][d)]	HOMO [eV][e)]	LUMO [eV][e)]
P1	25.7/1.63	453	4.7 (at 550 nm)	493	580	2.13	1.09	−5.42	−3.29
P2	32.7/1.75	488, 587	5.4 (at 585 nm)	581	633	1.96	1.21	−5.54	−3.58
P3	27.8/1.74	522, 566	5.7 (at 566 nm)	572	618	2.00	1.29	−5.62	−3.62

[a)]Measured by GPC; [b)]The molar extinction coefficient of the polymers in CF solution was measured using the Beer–Lambert law ($A = \varepsilon bc$); [c)]Estimated values from the UV–vis absorption edge of the thin film (E_g^{opt} = 1240/λ_{onset}, eV); [d)]The onset oxidation and reduction potentials were presented by reference to the redox potential of ferrocene/ferrocenium (Fc/Fc+) system; [e)]HOMO and LUMO energy levels of these polymers were estimated with the following equations: $E_{HOMO} = -[E_{ox}^{onset}$(vs Ag/AgCl) − $E_{1/2}$ of Fc/Fc$^+$(vs Ag/AgCl)] − 4.8 (eV) (Measured $E_{1/2}$ of Fc/Fc$^+$ (vs Ag/AgCl) = 0.47 eV) and LUMO = E_g^{opt} − HOMO eV.

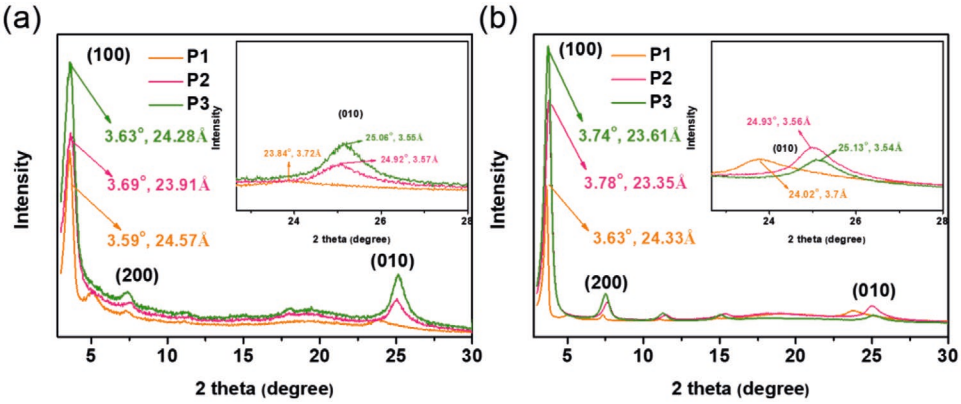

Figure 2. a) In-plane (q_{xy}) and b) out-of-plane (q_z) line cut profiles of the XRD images obtained from pristine P1–P3 polymers.

they also showed intense (010) peaks along q_{xy} and q_z, signifying the coexistence of bimodal, that is, edge-on and face-on, orientated semicrystalline domains. Notably, with the increase in the number of F substituents from P1 to P2 and then to P3, both fluorinated P2 and P3 polymers displayed intense (200) and (300) diffraction peaks along both directions with shorter lamellar stacking distances ($d_{(100)}q_{xy}/d_{(100)}q_z$ = 24.57/24.33 Å for P1 to 23.91/23.35 Å for P2 and 24.28/23.61 Å for P3) and π–π stacking *d*-spacing length ($d_{(010)}q_{xy}/d_{(100)}q_z$ = 3.72/3.70 Å for P1 to 3.57/3.56 Å for P2 and 3.55/3.54 Å for P3), implying both P2 and P3 exhibit higher crystallinity and more orderly molecular packing. In contrast, P1 showed the larger π–π stacking distances because of its twisted backbone, which led to low crystallinity. The higher crystallinity and favorable molecular ordering of P2 and P3 will aid in achieving higher carrier mobilities in OSCs, thereby assist in boosting J_{sc} and FF. These results further substantiate that the introduction of a fluorinated phenylene core in the molecular design is a significant approach for enhancing crystallinity in the resulting polymer via induction of stronger interchain packing, as reported previously.[34,48,50,59]

To gauge the potential of this series of polymers as donor materials for OSCs and to elucidate the effect of fluorination strategy on the molecular structure–property relationship, photovoltaic devices with an inverted device configuration of ITO/ZnO/polymer:IT-4F/MoO_3/Ag was fabricated. Initially, the systematic optimization of OSC device conditions was performed by optimizing the ratio of polymer:IT-4F and the processing solvents. As fluorination led to completely different aggregation behavior in the resulting copolymers, the optimized polymer concentration was found to be 10 mg mL^{-1} for P1 and 6.6 mg mL^{-1} for P2 and P3 in CF. Thermally annealed devices (100 °C for 10 min) with a polymer:IT-4F ratio of 1:1 (w/w) in CF yielded the best performance. The current density–voltage (*J*–*V*) curves of the various optimal photovoltaic devices are presented in **Figure 3**a, and the relative characteristics extracted from these curves are shown in **Table 2**. In this series, the optimized devices with fluorinated polymer donors P2 and P3 exhibited greatly enhanced PCEs of 6.89% (V_{oc} of 0.852 V, J_{sc} of 15.22 mA cm^{-2}, and FF of 53.1%) and 7.03% (V_{oc} of 0.96 V, J_{sc} of 13.00 mA cm^{-2}, and FF of 56.3%), respectively, compared to P1 with the lowest PCE of 0.16%. Notably, this enhancement of PCE resulted from radical enhancements and a good balance between all photovoltaic parameters compared to those in P1. The highest J_{sc} of ≈15.22 mA cm^{-2} of P2 is attributable to enhanced absorption, whereas the high V_{oc} of ≈0.96 V of P3 is due to its deep HOMO energy levels than those of the other polymers. Meanwhile, V_{oc} increased in the order P1 < P2 < P3, which is in good agreement with the low-lying HOMO energy levels caused by sequential fluorination. However, both P2- and P3-based optimal devices demonstrated lower FF values (<60%), which could be a consequence of the strong aggregation behaviors of P2 and P3, which subsequently hindered any

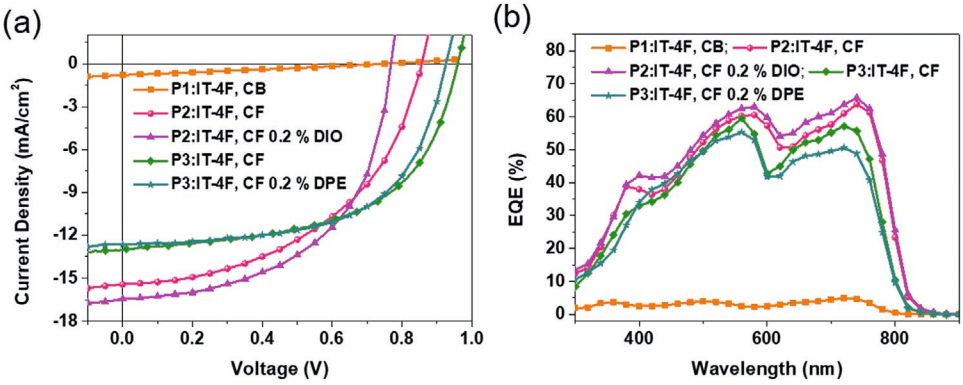

Figure 3. a) The *J*–*V* curves and b) EQE spectra of the optimized P1–P3:IT-4F solar cells with the best performance.

Table 2. Photovoltaic performance of the optimal OSCs based on the polymers:IT-4F (1:1, w/w) under different fabrication conditions.

Blend	V_{oc} [V]	J_{sc} [mA/cm^2]	FF [%]	PCE [%][a)]	E_g^{onset} [eV][e)]	E_{loss} [eV][f)]	μ_e [cm^2 V^{-1} s^{-1}][g)]	μ_h [cm^2 V^{-1} s^{-1}][h)]	μ_e/μ_h
P1:IT-4F[b)]	0.754	0.803	26.9	0.16 (0.15)	1.53	0.77	6.71×10^{-4}	9.93×10^{-6}	73.09
P2:IT-4F[b)]	0.852	15.22	53.1	6.89 (6.55)	1.50	0.65	8.57×10^{-4}	9.18×10^{-5}	9.33
P2:IT-4F[c)]	0.769	16.43	54.5	6.89 (6.62)	–	–	–	–	–
P3:IT-4F[b)]	0.960	13.00	56.3	7.03 (6.75)	1.51	0.55	9.31×10^{-4}	1.43×10^{-4}	6.51
P3:IT-4F[d)]	0.926	12.64	59.8	7.00 (6.68)	–	–	–	–	–

[a)]The best and the average results (4–6 devices) are tabulated outside and inside of the parentheses, respectively; [b)]Device processed with CF and thermal annealing at 100 °C for 10 min; [c)]Device processed with CF with 0.2% DIO and thermal annealing at 100 °C for 10 min; [d)]Device processed with CF with 0.2% DPE and thermal annealing at 100 °C for 10 min; [e)]E_g^{onset} is the optical gap of the main light absorber, which is calculated from EQE spectrum; [f)]$E_{loss} = E_g^{onset} - qV_{OC}$, where q is the elementary charge[29,30]; [g)]The hole-only device had the configuration ITO/PEDOT:PSS/active layer/MoO_3/Ag; [h)]The electron-only device had the configuration ITO/ZnO/active-layer/LiF/Al.

further enhancement in PCE relative to other high-efficiency PT-copolymers. Details regarding the optimization of P2- and P3-based devices are given in Figure S3 and Tables S3 and S4, Supporting Information. The EQE profiles of the best devices were measured to further probe the effectiveness of photon harvesting and verify the accuracy of the Jsc values obtained from the *J–V* curves. As shown in the EQE spectra in Figure 3b, both the P2- and P3-blend devices processed with/without solvent additives afforded a remarkably broad photoresponse range from 400–880 nm with larger EQE values exceeding 60% and 55%, respectively, in the 500–780 nm region, which suggests that strong and more complementary absorption of polymers and IT-4F is responsible for the observed effective light-harvesting and high *J*sc values. From the EQE curves, the calculated *J*sc values calculated for the devices without any additives were 0.91, 14.41, and 12.79 mA cm^{-2}, respectively, for P1–P3, which is in accordance with those obtained from the corresponding *J–V* measurements. Thus, enabled by the higher planarity and absorption coefficient, P2-based devices showed the best *J*sc values among the series.

Furthermore, the use of solvent additives is a proven technique to boost PCE by refining the crystalline phases and morphology of the resulting blend;[60,61] thus, we used 1,8-diiodooctane (DIO) or diphenyl ether (DPE) additives to further improve the PCEs of the P2 and P3 blend systems (Figures S4 and S5 and Tables S5 and S6, Supporting Information). With the addition of 0.2 vol% DIO in the solution of P2:IT-4F, J_{sc} and FF were increased from 15.22 to 16.43 mA cm^{-2} and 53.1% to 54.5%, respectively, with a slight decrease in V_{oc} from 0.852 to 0.769 V, leading to a PCE of 6.89%. Likewise, P3:IT-4F devices also produced the best PCE of 7.00% by the addition of 0.2 vol% DPE, where FF was slightly improved from 54.5% to 59.8%, and V_{oc} and J_{sc} were marginally lowered to 0.926 V and 12.64 mA cm^{-2}, respectively. We believe these changes were ascribed from the change in the micromorphology caused by changes in the crystallinity and interfacial area for effective charge separation, which in turn, critically affects J_{sc} and FF by changing individual phases of the blend components.[60–62] Besides, as discussed in the many reports, the drop in the V_{oc} mainly corresponds either to the improved crystallinity of the polymers caused by the low solubility of polymers in additives, thereby leading to the reduction in the effective bandgap estimated from the energetic onset of the charge-transfer band[62] or due to the decreased carriers lifetime/lower quasi-Fermi levels for both carriers caused by the depleted steady carriers density.[63,64] The EQE spectra of the devices with additives are shown in Figure 3b. Notably, the addition of 2 vol% DIO into P2:IT-4F devices resulted in enhanced light-to-current conversion along the whole wavelength region of the EQE spectra, thus justifying the highest J_{sc} compared to as-cast devices without any solvent additives (Figure 3a and Table 2). Next, realizing low E_{loss} is thought to be crucial to achieving high V_{oc} and photovoltaic performance in OSCs. From the E_g^{onset} of each combination (P1 or P2 or P3:ITIC-4F) and the V_{oc} values of the best devices, the relative E_{loss} values of the P1-, P2- and P3-based devices were estimated to be 0.77, 0.65, and 0.55 eV, respectively. Relative to P1 and P2, P3 displayed a considerably lower E_{loss} value of 0.55 eV, which is even smaller than the empirical threshold of 0.6 eV. Thus, both carboxylation and sequential fluorination aided in realizing lower E_{loss} values by lowering the ΔE_{HOMO} values from 0.26 eV for P1 to 0.14 eV for P2 and finally 0.05 eV for P3 via decreasing the HOMO energy levels.

Compared to P1-based OSCs without fluorination, di- and tetra-fluorinated P2- and P3-based OSCs exhibit drastically higher J_{sc} and FF values, which suggests that an in-depth analysis that investigates charge dissociation, carrier mobilities, and morphology is necessary to identify the dominant constraints responsible for the abysmal PCEs of P1. First, steady-state photoluminescence (PL) quenching of the optimized polymer:IT-4F-based blend devices were assessed to obtain information about the photo-induced charge transfer caused by the degree of phase separation. **Figure 4** represents the PL spectra of the pure polymers and IT-4F (excited at 490, 575, 575, and 720 nm for P1, P2, P3, and IT-4F, respectively) as well as the optimal polymer:IT-4F blend films (excited at 600 and 700 nm [P1:IT-4F] and 575 and 700 nm [P2 or P3:IT-4F]), and corresponding PL quenching efficiencies were tabulated in Table S7, Supporting Information. Notably, all three pristine polymer films have an intense PL emission band from 600–900 nm with ≈20 nm red-shift in comparison with their UV–vis absorption spectra. In contrast, these emission profiles were greatly quenched by over 90% for all of the polymer:IT-4F blends, implying that the electrons formed in the donor polymer were effectively dissociated into IT-4F (Figure 4a–c).[65,66] Similarly, all of the blend films were excited at 720 nm to estimate the efficiency of hole transfer from IT-4F to the corresponding polymer donors (Figure 4d–f). However, in this case of P1-, P2-, and P3-based blends, they presented a PL quenching rate of 76.8%, 93%, and 95.8%, respectively, versus

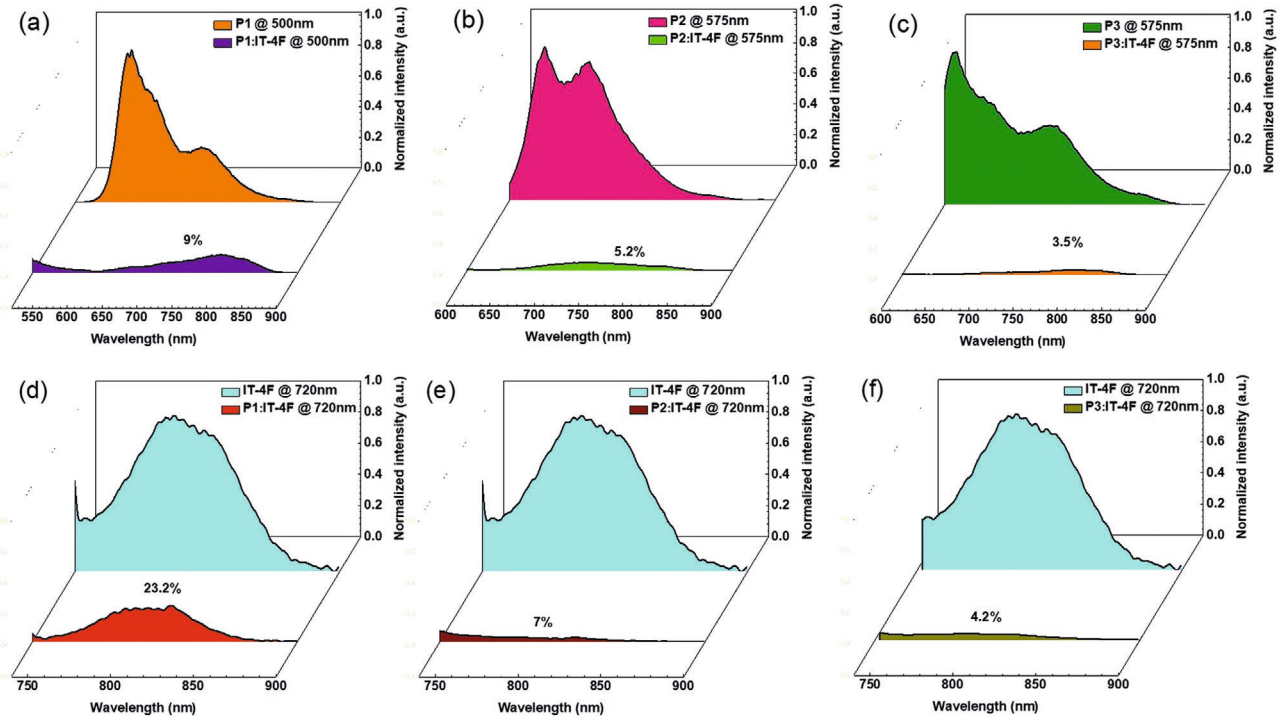

Figure 4. Photoluminescence spectra of the a) P1 (excited at 500 nm), b,c) P2 and P3 (excited at 575 nm), respectively, d) IT-4F (excited at 720 nm), as well as blend films of P1:IT-4F (excited at 500 and 720 nm) (a,d), P2:IT-4F (b,e) and P3:IT-4F (c,f), respectively (excited at 575 and 720 nm).

pristine IT-4F film, which indicates that the hole transfer rate of P1 is the poorest among all three polymers. The insufficient PL quenching suggests the ineffective transition from exciton to charge-transfer exciton, which may be related to the lower energy difference between E_g and energy of the charge-transfer state (E_{CT}) and/or slightly poor energy level alignment of the P1 and IT-4F as indicated in the previous studies,[67–69] and thereby emphasizing improving the BHJ morphologies is highly desirable to further enhance the J_{sc} in the corresponding devices. As a result, both P2:IT-4F- and P3:IT-4F-based devices displayed more effective charge dissociation and collection processes than P1:IT-4F blend films (where these processes were effective only in P1-rich domains and not in IT-4F-rich domains) and these findings correspond well with the J_{sc} values obtained from the optimized blend films.

Next, the hole (μ_h) and electron mobilities (μ_e) of the blend film were estimated using the space charge limited current technique to ascertain the effects of fluorination on J_{sc} and FF. As shown in Table 2 and the plots of $J^{1/2}$–V_{appl} (Figure S6, Supporting Information), μ_h was estimated to be 9.93×10^{-6}, 9.18×10^{-5}, and 1.43×10^{-4} cm^2 V^{-1} s^{-1} for P1-, P2-, and P3-based blend films, respectively. Among the devices, the P2- and P3-blend films displayed one and two orders higher μ_h, respectively, due to F-induced non-covalent intra/intermolecular interactions, which correlate well with their superior molecular ordering and shorter π–π stacking distance as revealed in the XRD study. In contrast, P1-based devices displayed inferior μ_h due to their weak π–π stacking and distortion of the copolymer backbone. μ_e also followed the same trend as μ_h. There was an increasing trend in the μ_e values from P1 to P3: 9.31×10^{-4} (P3) > 8.57×10^{-4} (P2) > 6.71×10^{-4} (P1) cm^2 V^{-1} s^{-1}, leading to relative μ_e/μ_h ratios of 73.09, 9.33, and 6.51, respectively. It is well-known that, along with higher charge carrier mobilities, a good balance between μ_e and μ_h is essential since this balance aids in reducing charge build-up at the interface, favoring higher FF and PCEs in the devices.[69,70] Considering the efficacy of exciton dissociation and high charge mobilities, it is evident that both fluorinated P2 and P3 displayed more balanced μ_e/μ_h values relative to their without-F counterpart P1, hence justifying the superior J_{sc} and PCE values of the corresponding optimized OSC devices. In contrast, owing to the lower and unbalanced charge carrier mobilities and hindered charge transport from IT-4F to P1 and poor morphology (discussed below), P1-based blends showed the lowest J_{sc}, FF, and PCE.

Since the BHJ morphology of the blend films is another critical determining factor for realizing effective exciton dissociation at the polymer/acceptor interfaces and charge transport in OSCs, the morphology of the blends in this series was also estimated using atomic force microscopy (AFM) and transmission electron microscopy (TEM). The AFM height images of the P1:IT-4F blend revealed a relatively smooth surface with a root-mean-square roughness (R_q) of 1.22 nm (**Figure 5**a). On the other hand, the P2:IT-4F and P3:IT-4F blends displayed rougher surfaces, with R_q of 1.70 and 2.04 nm, respectively (Figure 5b,c), which accords with the UV and XRD results, confirming that stronger interchain aggregation and enhanced crystallinity resulted from fluorination. These features could enhance the interfacial contact area between the active layer and the interfacial electrode, in turn improving charge collection. The TEM image in Figure 5d shows that the P1-based film exhibits a homogenous but featureless morphology that is made up of very small domains (<≈10 nm). As indicated in previous

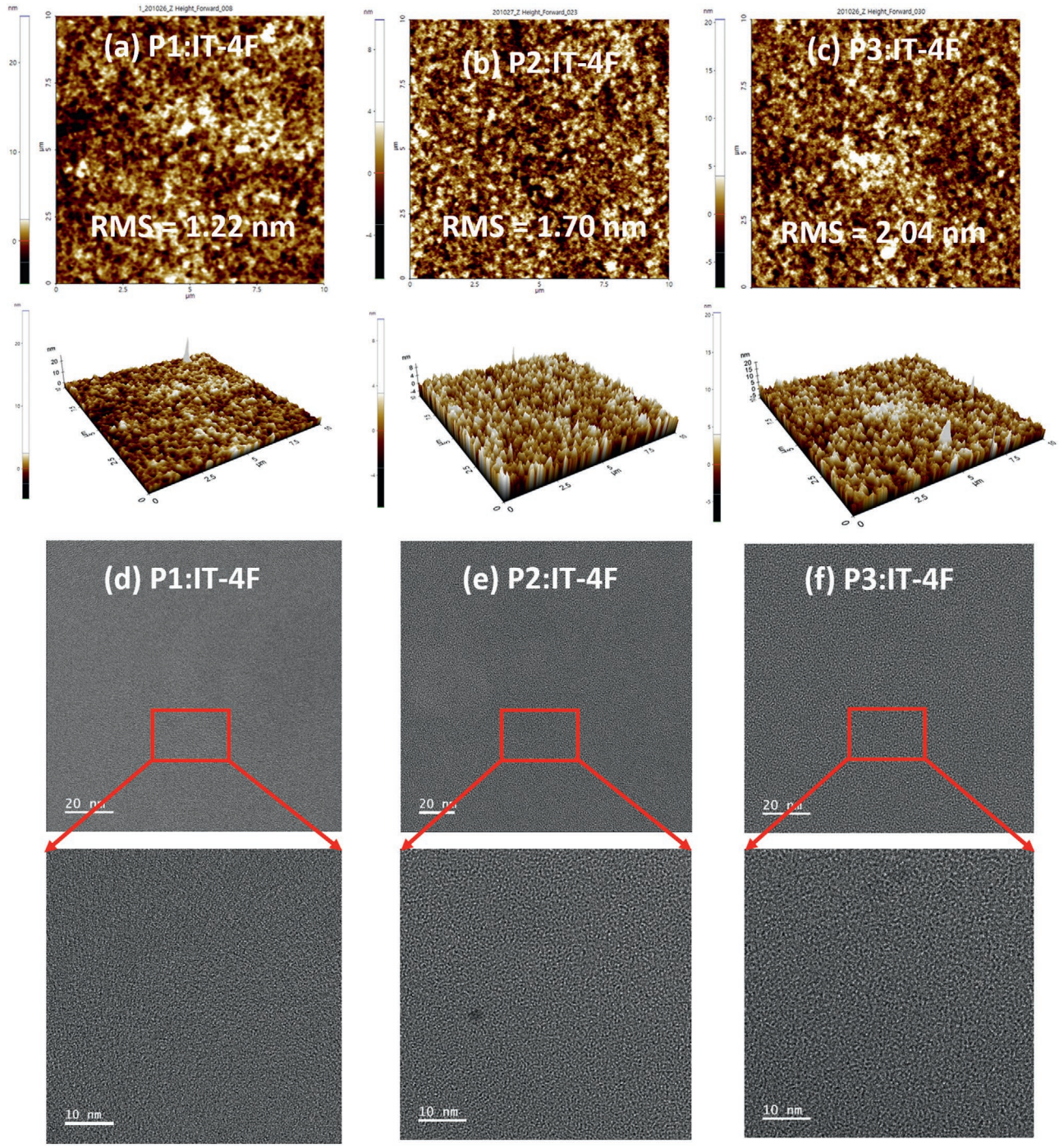

Figure 5. Tapping mode AFM a–c) topography (along with 3D images) and d–f) TEM images of optimal (a,d) P1:IT-4F, (b,e) P2:IT-4F and (c,f) P3:IT-4F blend films.

reports, such a small phase separation hinders the generation of charge carriers by lowering the exciton diffusion length and causes a drastic loss in photocurrent and FF by promoting charge recombination.[55,71] In the P2- and P3-based blends, domains become well-resolved and bicontinuous nano-fibrillar interpenetrating networks with finely distributed phase separation were unambiguously present (Figure 5e,f). Such phase-separated morphology can form well-developed D–A interfaces and well-percolated channels for effective dissociation and transport of the charge carriers by minimizing charge recombination, thus improving J_{SC} and FF. Overall, sequential fluorination of the phenylene units in the P2 and P3 backbone greatly improved the intermolecular interactions, molecular ordering, and nanoscale BHJ morphology with higher D–A interfacial

area, thereby affording efficient PL quenching, higher charge carrier mobilities, J_{sc}, FF, and PCE in the optimized devices. In contrast, as indicated by DFT, UV-absorption profiles, XRD, TEM, and the behavior of the P1-based devices, insertion of a phenylene moiety without any intermolecular interactions could induce distortion of the polymer backbone and weaken the molecular ordering while increasing the π–π stacking distance, which explains why the P1-based devices showed poor performance.

Overall, we tested the feasibility of replacing the critical halogenated bithiophene with phenylene moieties with a different amount of F in the reference PDCBT polymer donor. The study of opto–electrochemical properties and XRD analysis revealed that the new polymers exhibited a similar bandgap, deep-lying HOMO energy levels, and strong aggregation behavior when compared to halogenated PDCBT. Meanwhile, they also showed lower synthetic costs due to the lower raw materials cost, shorter synthetic steps, and easy purification of fluorinated phenylene precursors. The OSCs devices of these polymers were prepared by blending with IT-4F acceptor. The devices based on P2 and P3 showed the PCE of 6.89% and 7.03%, respectively, which is lower than previously reported reference PDCBT polymers. As expected, new polymers demonstrated high V_{oc} with remarkably low E_{loss} values, but they demonstrated marginally lower FF and J_{SC} due to the high aggregation tendencies of polymers caused by the synergistic carboxylation and fluorination. Because of the advantage of easy scalability of these polymers, further tests to improvise the FF and J_{SC} via decreasing the high aggregation by synthesizing terpolymers and optimizing the device fabrication conditions like using mixed solvents, solvent vapor annealing, and ternary OSCs is underway at present.

3. Conclusion

In conclusion, we reported three new dicarboxylate bithiophene-based WBG polymers, P1, P2 and P3, having phenylene cores with different numbers of F substituents (n = 0, 2, and 4, respectively) by facile synthetic routes with high yields. Enabled by the fluorination effect, both P2 and P3 possessed deeper HOMO energy levels, higher absorption coefficients, and more favorable molecular ordering with shorter π–π stacking distances than seen in their without F-counterpart P1. When blended with the non-fullerene IT-4F, both P2- and P3-based OSCs demonstrated PCEs as high as 6.89% and 7.03% with lower E_{loss} values from 0.65 to 0.55 eV, respectively, thereby vastly outperforming P1 (PCE of 0.15%). In addition to the planar molecular backbone, more effective complementary absorption and well-aligned energy level matching with IT-4F, higher and more well-balanced charge carrier mobilities, and optimal nanoscale morphology were other main reasons behind the superior PCEs of the P2- and P3-based OSCs. By contrast, P1 showed an extremely low PCE, mainly because of its twisted polymer backbone, which hampered its molecular ordering and intra/intermolecular charge transport in the corresponding OSCs. This systematic structure–property relationship provides valuable insights for the synthesis of efficient WBG polymers with increased V_{OC} via minimization of E_{loss} in OSCs.

Supporting Information

Supporting Information is available from the Wiley Online Library or from the author.

Acknowledgements

This research was supported by the New and Renewable Energy Core Technology Program (No. 20193091010110) and Human Resources program in Energy Technology (No. 20194010201790) of the Korean Institute of Energy Technology Evaluation and Planning (KETEP) grant funded by the Ministry of Trade, Industry and Energy, Republic of Korea. This work was supported by the National Research Foundation of Korea (NRF) grant funded by the Korea government (MSIT) (No. 2020R1A2C201091611). This research was supported by the 2020 KU Brain Pool of Konkuk University, Korea.

Conflict of Interest

The authors declare no conflict of interest.

Data Availability Statement

Research data are not shared.

Keywords

fluorinated phenylene moieties, fluorine effect, high open-circuit voltage, low photon energy loss, non-fullerene organic solar cells

Received: December 18, 2020
Revised: January 14, 2021
Published online: March 1, 2021

[1] A. J. Heeger, *Adv. Mater.* **2014**, *26*, 10.
[2] L. Lu, T. Zheng, Q. Wu, A. M. Schneider, D. Zhao, L. Yu, *Chem. Rev.* **2015**, *115*, 12666.
[3] R. Xue, J. Zhang, Y. Li, Y. Li, *Small* **2018**, *14*, 1801793.
[4] Y. Lin, Y. Jin, S. Dong, W. Zheng, J. Yang, A. Liu, F. Liu, Y. Jiang, T. P. Russell, F. Zhang, F. Huang, L. Hou, *Adv. Energy Mater.* **2018**, *8*, 1701942.
[5] Y. Li, G. Xu, C. Cui, Y. Li, *Adv. Energy Mater.* **2018**, *8*, 1701791.
[6] T. Yan, W. Song, J. Huang, R. Peng, L. Huang, Z. Ge, *Adv. Mater.* **2019**, *31*, 1902210.
[7] C. An, Z. Zheng, J. Hou, *Chem. Commun.* **2020**, *56*, 4750.
[8] X. Xu, G. Zhang, Y. Li, Q. Peng, *Chin. Chem. Lett.* **2019**, *30*, 809.
[9] G. P. Kini, S. J. Jeon, D. K. Moon, *Adv. Mater.* **2020**, *32*, 1906175.
[10] H. Fu, Z. Wang, Y. Sun, *Angew. Chem., Int. Ed.* **2019**, *58*, 4442.
[11] S. Li, C.-Z. Li, M. Shi, H. Chen, *ACS Energy Lett.* **2020**, *5*, 1554.
[12] S. Dey, *Small* **2019**, *15*, 1900134.
[13] Z. Zhang, J. Yuan, Q. Wei, Y. Zou, *Front. Chem.* **2018**, *6*, 414.
[14] G. Zhang, J. Zhao, P. C. Y. Chow, K. Jiang, J. Zhang, Z. Zhu, J. Zhang, F. Huang, H. Yan, *Chem. Rev.* **2018**, *118*, 3447.
[15] C. Li, H. Fu, T. Xia, Y. Sun, *Adv. Energy Mater.* **2019**, *9*, 1900999.
[16] H. Wang, J. Cao, J. Yu, Z. Zhang, R. Geng, L. Yang, W. Tang, *J. Mater. Chem. A* **2019**, *7*, 4313.
[17] Y. Cui, H. Yao, J. Zhang, T. Zhang, Y. Wang, L. Hong, K. Xian, B. Xu, S. Zhang, J. Peng, Z. Wei, F. Gao, J. Hou, *Nat. Commun.* **2019**, *10*, 2515.

[18] R. Yu, H. Yao, Y. Cui, L. Hong, C. He, J. Hou, *Adv. Mater.* **2019**, *31*, 1902302.
[19] X. Xu, K. Feng, Z. Bi, W. Ma, G. Zhang, Q. Peng, *Adv. Mater.* **2019**, *31*, 1901872.
[20] B. Fan, D. Zhang, M. Li, W. Zhong, Z. Zeng, L. Ying, F. Huang, Y. Cao, *Sci. China Chem.* **2019**, *62*, 746.
[21] Y. Cui, H. Yao, L. Hong, T. Zhang, Y. Tang, B. Lin, K. Xian, B. Gao, C. An, P. Bi, W. Ma, J. Hou, *Natl. Sci. Rev.* **2019**, *7*, 1239.
[22] Q. Liu, Y. Jiang, K. Jin, J. Qin, J. Xu, W. Li, J. Xiong, J. Liu, Z. Xiao, K. Sun, S. Yang, X. Zhang, L. Ding, *Sci. Bull.* **2020**, *65*, 272.
[23] Y.-J. Hwang, B. A. E. Courtright, A. S. Ferreira, S. H. Tolbert, S. A. Jenekhe, *Adv. Mater.* **2015**, *27*, 4578.
[24] F. Cai, H. Peng, H. Chen, J. Yuan, J. Hai, T.-K. Lau, J. Wang, Y. Hu, W. Liu, X. Lu, Y. Zou, *J. Mater. Chem. A* **2020**, *8*, 15984.
[25] Q. He, M. Shahid, J. Wu, X. Jiao, F. D. Eisner, T. Hodsden, Z. Fei, T. D. Anthopoulos, C. R. McNeill, J. R. Durrant, M. Heeney, *Adv. Funct. Mater.* **2019**, *29*, 1904956.
[26] J.-D. Chen, Y.-Q. Li, J. Zhu, Q. Zhang, R.-P. Xu, C. Li, Y.-X. Zhang, J.-S. Huang, X. Zhan, W. You, J.-X. Tang, *Adv. Mater.* **2018**, *30*, 1706083.
[27] T. Liu, L. Huo, S. Chandrabose, K. Chen, G. Han, F. Qi, X. Meng, D. Xie, W. Ma, Y. Yi, J. M. Hodgkiss, F. Liu, J. Wang, C. Yang, Y. Sun, *Adv. Mater.* **2018**, *30*, 1707353.
[28] Z. Zheng, Q. Hu, S. Zhang, D. Zhang, J. Wang, S. Xie, R. Wang, Y. Qin, W. Li, L. Hong, N. Liang, F. Liu, Y. Zhang, Z. Wei, Z. Tang, T. P. Russell, J. Hou, H. Zhou, *Adv. Mater.* **2018**, *30*, 1801801.
[29] Y. Tang, H. Sun, Z. Wu, Y. Zhang, G. Zhang, M. Su, X. Zhou, X. Wu, W. Sun, X. Zhang, B. Liu, W. Chen, Q. Liao, H. Y. Woo, X. Guo, *Adv. Sci.* **2019**, *6*, 1901773.
[30] C. Wang, X. Xu, W. Zhang, J. Bergqvist, Y. Xia, X. Meng, K. Bini, W. Ma, A. Yartsev, K. Vandewal, M. R. Andersson, O. Inganäs, M. Fahlman, E. Wang, *Adv. Energy Mater.* **2016**, *6*, 1600148.
[31] Z. Yao, X. Liao, K. Gao, F. Lin, X. Xu, X. Shi, L. Zuo, F. Liu, Y. Chen, A. K. Y. Jen, *J. Am. Chem. Soc.* **2018**, *140*, 2054.
[32] H. Yao, Y. Cui, D. Qian, C. S. Ponseca, A. Honarfar, Y. Xu, J. Xin, Z. Chen, L. Hong, B. Gao, R. Yu, Y. Zu, W. Ma, P. Chabera, T. Pullerits, A. Yartsev, F. Gao, J. Hou, *J. Am. Chem. Soc.* **2019**, *141*, 7743.
[33] S. Li, L. Ye, W. Zhao, H. Yan, B. Yang, D. Liu, W. Li, H. Ade, J. Hou, *J. Am. Chem. Soc.* **2018**, *140*, 7159.
[34] Q. Wang, M. Li, X. Zhang, Y. Qin, J. Wang, J. Zhang, J. Hou, R. A. J. Janssen, Y. Geng, *Macromolecules* **2019**, *52*, 4464.
[35] Y. Kim, S. Cook, S. M. Tuladhar, S. A. Choulis, J. Nelson, J. R. Durrant, D. D. C. Bradley, M. Giles, I. McCulloch, C.-S. Ha, M. Ree, *Nat. Mater.* **2006**, *5*, 197.
[36] G. Li, V. Shrotriya, J. Huang, Y. Yao, T. Moriarty, K. Emery, Y. Yang, *Nat. Mater.* **2005**, *4*, 864.
[37] S. Holliday, R. S. Ashraf, A. Wadsworth, D. Baran, S. A. Yousaf, C. B. Nielsen, C.-H. Tan, S. D. Dimitrov, Z. Shang, N. Gasparini, M. Alamoudi, F. Laquai, C. J. Brabec, A. Salleo, J. R. Durrant, I. McCulloch, *Nat. Commun.* **2016**, *7*, 11585.
[38] L. Huo, T. L. Chen, Y. Zhou, J. Hou, H.-Y. Chen, Y. Yang, Y. Li, *Macromolecules* **2009**, *42*, 4377.
[39] M. Zhang, X. Guo, W. Ma, H. Ade, J. Hou, *Adv. Mater.* **2014**, *26*, 5880.
[40] M. Zhang, X. Guo, Y. Yang, J. Zhang, Z.-G. Zhang, Y. Li, *Polym. Chem.* **2011**, *2*, 2900.
[41] Z. Liang, M. Li, Q. Wang, Y. Qin, S. J. Stuard, Z. Peng, Y. Deng, H. Ade, L. Ye, Y. Geng, *Joule* **2020**, *4*, 1278.
[42] Y. Qin, M. A. Uddin, Y. Chen, B. Jang, K. Zhao, Z. Zheng, R. Yu, T. J. Shin, H. Y. Woo, J. Hou, *Adv. Mater.* **2016**, *28*, 9416.
[43] H. Zhang, S. Li, B. Xu, H. Yao, B. Yang, J. Hou, *J. Mater. Chem. A* **2016**, *4*, 18043.
[44] S.-J. Ko, Q. V. Hoang, C. E. Song, M. A. Uddin, E. Lim, S. Y. Park, B. H. Lee, S. Song, S.-J. Moon, S. Hwang, P.-O. Morin, M. Leclerc, G. M. Su, M. L. Chabinyc, H. Y. Woo, W. S. Shin, J. Y. Kim, *Energy Environ. Sci.* **2017**, *10*, 1443.
[45] Y.-J. You, C. E. Song, Q. V. Hoang, Y. Kang, J. S. Goo, D.-H. Ko, J.-J. Lee, W. S. Shin, J. W. Shim, *Adv. Funct. Mater.* **2019**, *29*, 1901171.
[46] J. Zhao, Y. Li, G. Yang, K. Jiang, H. Lin, H. Ade, W. Ma, H. Yan, *Nat. Energy* **2016**, *1*, 15027.
[47] Q. Zhang, M. A. Kelly, N. Bauer, W. You, *Acc. Chem. Res.* **2017**, *50*, 2401.
[48] J. Yang, M. A. Uddin, Y. Tang, Y. Wang, Y. Wang, H. Su, R. Gao, Z.-K. Chen, J. Dai, H. Y. Woo, X. Guo, *ACS Appl. Mater. Interfaces* **2018**, *10*, 23235.
[49] Q. Fan, U. A. Méndez-Romero, X. Guo, E. Wang, M. Zhang, Y. Li, *Chem. - Asian J.* **2019**, *14*, 3085.
[50] G. P. Kini, J. Y. Choi, S. J. Jeon, I. S. Suh, D. K. Moon, *Polymer* **2018**, *148*, 330.
[51] J. Yuan, Y. Zhang, L. Zhou, G. Zhang, H.-L. Yip, T.-K. Lau, X. Lu, C. Zhu, H. Peng, P. A. Johnson, M. Leclerc, Y. Cao, J. Ulanski, Y. Li, Y. Zou, *Joule* **2019**, *3*, 1140.
[52] G. P. Kini, H. S. Park, S. J. Jeon, Y. W. Han, D. K. Moon, *Sol. Energy* **2020**, *207*, 720.
[53] T. Wang, J. Qin, Z. Xiao, J. Zhang, Z. Chen, L. Zhang, M. Cheng, Z. Jin, Y. Yuan, W.-Q. Wu, C. Duan, S. Xie, K. Sun, F. Hao, L. Ding, *Nano Energy* **2020**, *77*, 105161.
[54] J. E. Yu, S. J. Jeon, J. Y. Choi, Y. W. Han, E. J. Ko, D. K. Moon, *Small* **2019**, *15*, 1805321.
[55] P. Chao, L. Liu, J. Zhou, J. Qu, D. Mo, H. Meng, Z. Xie, F. He, Y. Ma, *ACS Appl. Energy Mater.* **2018**, *1*, 6549.
[56] K. D. Deshmukh, R. Matsidik, S. K. K. Prasad, N. Chandrasekaran, A. Welford, L. A. Connal, A. C. Y. Liu, E. Gann, L. Thomsen, D. Kabra, J. M. Hodgkiss, M. Sommer, C. R. McNeill, *ACS Appl. Mater. Interfaces* **2018**, *10*, 955.
[57] S. Chen, H. Yao, Z. Li, O. M. Awartani, Y. Liu, Z. Wang, G. Yang, J. Zhang, H. Ade, H. Yan, *Adv. Energy Mater.* **2017**, *7*, 1602304.
[58] T. Duan, J. Gao, T. Xu, Z. Kan, W. Chen, R. Singh, G. P. Kini, C. Zhong, D. Yu, Z. Xiao, Z. Xiao, S. Lu, *J. Mater. Chem. A* **2020**, *8*, 5843.
[59] K. Kawashima, T. Fukuhara, Y. Suda, Y. Suzuki, T. Koganezawa, H. Yoshida, H. Ohkita, I. Osaka, K. Takimiya, *J. Am. Chem. Soc.* **2016**, *138*, 10265.
[60] X. Song, N. Gasparini, D. Baran, *Adv. Electron. Mater.* **2018**, *4*, 1700358.
[61] Y. Gao, R. Zhu, Z. Wang, F. Guo, Z. Wei, Y. Yang, L. Zhao, Y. Zhang, *ACS Appl. Energy Mater.* **2018**, *1*, 1888.
[62] J. Kim, J.-S. Yeo, H.-G. Jeong, J.-M. Yun, Y.-A. Kim, D.-Y. Kim, *Sol. Energy Mater. Sol. Cells* **2014**, *125*, 253.
[63] X. Wang, Y. Yang, Z. He, H. Wu, Y. Cao, *J. Mater. Chem. C* **2019**, *7*, 14861.
[64] S. Xie, J. Wang, R. Wang, D. Zhang, H. Zhou, Y. Zhang, D. Zhou, *Chin. Chem. Lett.* **2019**, *30*, 217.
[65] G. P. Kini, J. Y. Choi, S. J. Jeon, I. S. Suh, D. K. Moon, *Dyes Pigm.* **2019**, *164*, 62.
[66] S. H. Park, G. E. Park, S. Choi, Y. U. Kim, S. Y. Park, C. G. Park, M. J. Cho, D. H. Choi, *J. Mater. Chem. C* **2018**, *6*, 7549.
[67] L. Hong, H. Yao, R. Yu, Y. Xu, B. Gao, Z. Ge, J. Hou, *ACS Appl. Mater. Interfaces* **2019**, *11*, 29124.
[68] K. Nakano, Y. Chen, B. Xiao, W. Han, J. Huang, H. Yoshida, E. Zhou, K. Tajima, *Nat. Commun.* **2019**, *10*, 2520.
[69] D. Liu, B. Yang, B. Jang, B. Xu, S. Zhang, C. He, H. Y. Woo, J. Hou, *Energy Environ. Sci.* **2017**, *10*, 546.
[70] G. P. Kini, S. R. Suranagi, M. Kumar, R. Singh, *Dyes Pigm.* **2020**, *175*, 108083.
[71] G. P. Kini, J. Y. Choi, S. J. Jeon, I. S. Suh, D. K. Moon, *Polym. Chem.* **2019**, *10*, 4459.
[72] G. P. Kini, S. J. Jeon, D. K. Moon, *Advanced Functional Materials* **2021**, 2007931. http://doi.org/10.1002/adfm.202007931.